Optical properties of fourteen metals in the infrared and far infrared: Al, Co, Cu, Au, Fe, Pb, Mo, Ni, Pd, Pt, Ag, Ti, V, and W.

M. A. Ordal, Robert J. Bell, R. W. Alexander, Jr, L. L. Long, and M. R. Querry

Infrared optical constants collected from the literature are tabulated for Mo and V. New data are presented for Cu, Fe, and Ni. Drude model parameters ω_τ and ω_p are given for the fourteen metals Al, Co, Cu, Au, Fe, Pb, Mo, Ni, Pd, Pt, Ag, Ti, V, and W. The Drude model parameters for Cu are revised from our earlier tabulation due to the availability of additional data. Refinements in our fitting technique have resulted in only slight changes in the Drude model parameters for Al, Au, Ag, and W. The Drude model parameters for Pb correct a numerical error in our earlier tabulation. For all fourteen metals, the optical resistivity has been calculated from the Drude model parameters ω_τ and ω_p and compared to handbook values for the dc resistivity.

I. Introduction

In our earlier tabulation of the optical constants of twelve metals[1] we showed that the Drude model provided a useful parametrization for the optical constants of six metals; Al, Cu, Au, Pb, Ag, and W. Since then we have parametrized the other six metals in our earlier tabulation; Fe, Co, Ni, Pd, Pt, and Ti. We have expanded our earlier tabulation by adding data on Mo and V from Weaver *et al.*[2]; our recently acquired data on Cu, Fe, and Ni; and data on V from Johnson and Christy.[3]

In general, the Drude model is not expected to be appropriate for transition metals in the near IR. Nevertheless, a Drude model parametrization of the dielectric function is a useful approximation (sometimes over a surprisingly large frequency range) for these metals.

II. Definitions

In keeping with IR spectroscopic notation, all frequencies will be expressed in cm^{-1}. The complex dielectric function ϵ_c and the complex index of refraction n_c are defined as [1]

$$\epsilon_c \equiv \epsilon_1 + i\epsilon_2 \equiv {n_c}^2 \equiv (n + ik)^2. \tag{1}$$

The Drude model dielectric function is

$$\epsilon_c = \epsilon_\infty - \frac{{\omega_p}^2}{\omega^2 + i\omega\omega_\tau}, \tag{2}$$

where ω, ω_p, and ω_τ have units of cm^{-1}. Separating real and imaginary parts yields

$$\epsilon_1 = \epsilon_\infty - \frac{{\omega_p}^2}{\omega^2 + {\omega_\tau}^2}, \tag{3}$$

$$\epsilon_2 = \frac{\omega_\tau {\omega_p}^2}{\omega(\omega^2 + {\omega_\tau}^2)}. \tag{4}$$

In these equations, the plasma frequency is

$$\omega_p(\text{cm}^{-1}) = \frac{1}{2\pi c}\left(\frac{4\pi N e^2}{m^*}\right)^{1/2}, \tag{5}$$

where in cgs units N is the free electron density, e is the electronic charge, m^* is the effective mass of the electrons, and c is the speed of light in vacuum. Equation (5) corrects the like numbered equation in our earlier publication.[1]

The damping frequency ω_τ is

$$\omega_\tau(\text{cm}^{-1}) = \frac{1}{2\pi c\tau}, \tag{6}$$

where τ is the electron lifetime in seconds.

The high or optical frequency conductivity σ_{opt} is related to ω_p and ω_τ by

$$\sigma_{\text{opt}} = \frac{{\omega_p}^2}{4\pi\omega_\tau}, \tag{7}$$

where σ_{opt} has units of cm^{-1}. This optical conductiv-

M. R. Querry is with University of Missouri-Kansas City, Physics Department, Kansas City, Missouri 64110; the other authors are with University of Missouri-Rolla, Physics Department, Rolla, Missouri 65401.

Received 11 June 1985.
0003-6935/85/244493-07$02.00/0.

ity should also be equal to the dc conductivity which can be expressed in terms of the dc resistivity ρ_0:

$$\sigma_0(\mathrm{cm}^{-1}) = \frac{1}{2\pi c[\rho_0(\mathrm{sec})]} = \frac{9 \times 10^{11}}{2\pi c[\rho_0(\Omega\mathrm{cm})]} . \tag{8}$$

We note that these two conductivities are not always equal as can later be seen in Table I.

Using the sign convention adopted in Eq. (1) we can write the surface impedance, $Z(\omega) \equiv R(\omega) + iX(\omega)$, for the Drude model:

$$Z(\omega) = \frac{4\pi}{c}(1-i)\sqrt{\left(\frac{\omega\omega_\tau}{2\omega_p^2}\right)\left(1 - \frac{i\omega}{\omega_\tau}\right)} . \tag{9}$$

Extracting the real and imaginary parts we get

$$R(\omega) = \frac{4\pi}{c}\sqrt{\frac{\omega\omega_\tau}{2\omega_p^2}}\left(\frac{-\omega}{\omega_\tau} + \sqrt{1 + \frac{\omega^2}{\omega_\tau^2}}\right)^{1/2} . \tag{10}$$

$$X(\omega) = \frac{-4\pi}{c}\sqrt{\frac{\omega\omega_\tau}{2\omega_p^2}}\left(\frac{\omega}{w_\tau} + \sqrt{1 + \frac{\omega^2}{\omega_\tau^2}}\right)^{1/2} . \tag{11}$$

Taking the other sign convention (i.e., $n - ik$) leaves the expression for $R(\omega)$ unchanged, multiplies the expression for $X(\omega)$ by -1, and replaces $-i$ by i in the expression for $Z(\omega)$. Equation (9) corrects Eq. (10) in our earlier publication.[1] Since Eq. (10) remains the same for either sign convention, the numerical results given in our Ref. 1 remain unchanged.

III. Determination of Drude Model Parameters

Equations (3) and (4) can be solved for[1] for ω_τ to obtain

$$\omega_\tau = \frac{\omega\epsilon_2}{(\epsilon_\infty - \epsilon_1)} . \tag{12}$$

Equation (12) was used to obtain ω_τ using ϵ_1 and ϵ_2 at some frequency ω. Then ω_p was obtained from

$$\omega_p^2 = (\epsilon_\infty - \epsilon_1)(\omega^2 + \omega_\tau^2). \tag{13}$$

Equations (12) and (13) were applied to the lowest frequency data with ϵ_∞ taken to be unity.

We attempted to refine the values for ω_τ and ω_p obtained with the aforementioned method by fitting a function of ϵ_1 and ϵ_2. We tried various functions including ϵ_1/ϵ_2, ϵ_2/ϵ_1, $\epsilon_1\epsilon_2$ and $|\epsilon_c|$. The function $|\epsilon_c|$ worked better than the others but was surpassed slightly by the similar function

$$\sqrt{(\epsilon_1 - \epsilon_\infty)^2 + \epsilon_2^2} = \frac{\omega_p^2}{\omega^2 + \omega_\tau^2}\sqrt{1 + \left(\frac{\omega_\tau}{\omega}\right)^2} . \tag{14}$$

In cases where the data did not extend to frequencies both higher and lower than ω_τ, this fit method returned reasonable results in only a few cases. A major problem seems to be the large (orders of magnitude) difference in the values of $-\epsilon_1$ and ϵ_2 at frequencies away from ω_τ. It should be noted that a formal fit method worked well in those cases where data extend to frequencies both higher and lower than ω_τ. However, in such cases it is more convenient to obtain the value of ω_τ from Eqs. (3) and (4) with $\omega = \omega_\tau$. That is

$$-\epsilon_1 = \epsilon_2 - \epsilon_\infty \ (\text{for } \omega = \omega_\tau). \tag{15}$$

Table I. Results of a Drude Model Fit to the Dielectric Function of Fourteen Metals.[a]

Metal	$10^{-2}\omega_\tau$ (cm^{-1})	$10^{-4}\omega_p$ (cm^{-1})	ρ_{opt} ($\mu\Omega$ cm)	ρ_0[a] ($\mu\Omega$ cm)	ρ_0/ρ_{opt}
Al	6.60	11.9	2.80	2.74	0.98
Co	2.95	3.20	17.3	5.80	0.34
Cu	0.732	5.96	1.24	1.70	1.3
Au	2.15	7.28	2.43	2.20	0.91
Fe	1.47	3.30	8.10	9.80	1.20
Pb	16.3	5.94	27.7	21.0	0.76
Mo	4.12	6.02	6.82	5.33	0.78
Ni	3.52	3.94	13.3	7.04	0.52
Pd	1.24	4.40	3.84	10.55	2.8
Pt	5.58	4.15	19.4	10.42	0.54
Ag	1.45	7.27	1.65	1.61	0.98
Ti	3.82	2.03	55.6	43.1	0.78
V	4.89	4.16	17.0	19.9	1.2
W	4.87	5.17	10.9	5.33	0.49

[a] Ref. 5, pp. 9-39,9-40.

With ω_τ known, either ϵ_1 or ϵ_2 can be fit to obtain ω_p (although ϵ_1 is preferred since it tends to closely fit the Drude model to higher frequencies than ϵ_2).

Our fits are good enough for us to conclude that ϵ_∞ is much less than ϵ_1 or ϵ_2—that is, ϵ_∞ does not need to be taken as a third adjustable parameter in the fitting process.

The fit method used to obtain the values given in Table I remains a trial and error eyeball technique. The values of ω_τ and ω_p obtained from the lowest frequency data were changed by trial and error to obtain curves most closely matching the data for $-\epsilon_1$ and ϵ_2 in both magnitude and slope. In certain cases the need for lower frequency data is readily apparent. In such cases (e.g., Pd) the Drude model fit gives a reasonable estimate for $-\epsilon_1$ but not for ϵ_2. In other cases band structure, combined with a lack of very low frequency data, limits the Drude model fit to a fairly narrow frequency range (e.g.,Ti).

IV. Data

For our own measurements on Cu, Fe, and Ni the power reflectance was measured using an Al mirror as a standard. The measured reflectance of the samples was corrected for the absolute reflectance of this particular Al mirror using values measured by us. A Perkin-Elmer 580 was used in the 180–4000-cm^{-1} range, and a Varian model 2300 was used for the 4000–50,000-cm^{-1} range.

The Kramers-Kronig analysis of the reflectance data yielded n and k from which ϵ_1 and ϵ_2 were calculated. High and low frequency wing corrections were handled in various ways. At the low end we tried a constant wing where the zero frequency reflectance was assumed to equal the measured reflectance at 180 cm^{-1}. For the low frequency wing correction, we also tried a Drude model extrapolation down to 1 cm^{-1} and assumed a constant reflectance below 1 cm^{-1}. The Drude model parameters used for the low wing were found by trial and error starting with the values that best fit the higher frequency results of others. Trial and error adjustment of ω_τ and ω_p was necessary to

Table II. Copper

ω (cm^{-1})	λ (μm)	$-\epsilon_1$	ϵ_2	n	k
1.80E + 2	5.56E + 1	9.40E + 4	3.83E + 4	6.12E + 1	3.13E + 2
2.00E + 2	5.00E + 1	7.82E + 4	2.84E + 4	5.00E + 1	2.84E + 2
2.20E + 2	4.55E + 1	6.47E + 4	2.11E + 4	4.09E + 1	2.58E + 2
2.40E + 2	4.17E + 1	5.53E + 4	1.72E + 4	3.62E + 1	2.38E + 2
2.60E + 2	3.85E + 1	4.70E + 4	1.40E + 4	3.19E + 1	2.19E + 2
2.80E + 2	3.57E + 1	4.06E + 4	1.16E + 4	2.85E + 1	2.03E + 2
3.00E + 2	3.33E + 1	3.54E + 4	9.74E + 3	2.57E + 1	1.90E + 2
3.20E + 2	3.13E + 1	3.11E + 4	8.31E + 3	2.34E + 1	1.78E + 2
3.40E + 2	2.94E + 1	2.74E + 4	7.37E + 3	2.21E + 1	1.67E + 2
3.60E + 2	2.78E + 1	2.46E + 4	6.65E + 3	2.10E + 1	1.58E + 2
3.80E + 2	2.63E + 1	2.22E + 4	5.86E + 3	1.95E + 1	1.50E + 2
4.00E + 2	2.50E + 1	1.99E + 4	5.43E + 3	1.91E + 1	1.42E + 2
4.20E + 2	2.38E + 1	1.81E + 4	4.99E + 3	1.84E + 1	1.36E + 2
4.40E + 2	2.27E + 1	1.66E + 4	4.59E + 3	1.77E + 1	1.30E + 2
4.60E + 2	2.17E + 1	1.52E + 4	4.22E + 3	1.70E + 1	1.24E + 2
4.80E + 2	2.08E + 1	1.40E + 4	4.02E + 3	1.68E + 1	1.20E + 2
5.00E + 2	2.00E + 1	1.30E + 4	3.73E + 3	1.62E + 1	1.15E + 2
5.50E + 2	1.82E + 1	1.09E + 4	3.24E + 3	1.54E + 1	1.05E + 2
6.00E + 2	1.67E + 1	9.34E + 3	2.87E + 3	1.47E + 1	9.77E + 1
6.50E + 2	1.54E + 1	8.11E + 3	2.52E + 3	1.38E + 1	9.11E + 1
7.00E + 2	1.43E + 1	7.15E + 3	2.25E + 3	1.32E + 1	8.56E + 1
7.50E + 2	1.33E + 1	6.37E + 3	1.97E + 3	1.22E + 1	8.08E + 1
8.00E + 2	1.25E + 1	5.72E + 3	1.74E + 3	1.14E + 1	7.65E + 1
8.50E + 2	1.18E + 1	5.17E + 3	1.53E + 3	1.05E + 1	7.26E + 1
9.00E + 2	1.11E + 1	4.67E + 3	1.35E + 3	9.77E + 0	6.91E + 1
9.50E + 2	1.05E + 1	4.26E + 3	1.19E + 3	9.00E + 0	6.59E + 1
1.00E + 3	1.00E + 1	3.90E + 3	1.05E + 3	8.31E + 0	6.30E + 1
1.10E + 3	9.09E + 0	3.27E + 3	8.31E + 2	7.21E + 0	5.77E + 1
1.20E + 3	8.33E + 0	2.79E + 3	6.85E + 2	6.43E + 0	5.32E + 1
1.30E + 3	7.69E + 0	2.42E + 3	5.68E + 2	5.74E + 0	4.95E + 1
1.40E + 3	7.14E + 0	2.11E + 3	4.71E + 2	5.10E + 0	4.62E + 1
1.50E + 3	6.67E + 0	1.85E + 3	3.95E + 2	4.57E + 0	4.33E + 1
1.60E + 3	6.25E + 0	1.64E + 3	3.38E + 2	4.16E + 0	4.07E + 1
1.70E + 3	5.88E + 0	1.45E + 3	2.95E + 2	3.84E + 0	3.83E + 1
1.80E + 3	5.56E + 0	1.30E + 3	2.65E + 2	3.65E + 0	3.63E + 1
1.90E + 3	5.26E + 0	1.18E + 3	2.39E + 2	3.45E + 0	3.45E + 1
2.00E + 3	5.00E + 0	1.08E + 3	2.15E + 2	3.26E + 0	3.30E + 1
2.25E + 3	4.44E + 0	8.21E + 2	1.49E + 2	2.58E + 0	2.88E + 1
2.50E + 3	4.00E + 0	6.98E + 2	1.19E + 2	2.25E + 0	2.65E + 1
2.75E + 3	3.64E + 0	5.83E + 2	9.60E + 1	1.98E + 0	2.42E + 1
3.00E + 3	3.33E + 0	4.93E + 2	7.90E + 1	1.77E + 0	2.23E + 1
3.25E + 3	3.08E + 0	4.22E + 2	6.67E + 1	1.62E + 0	2.06E + 1
3.50E + 3	2.86E + 0	3.63E + 2	5.57E + 1	1.46E + 0	1.91E + 1
3.75E + 3	2.67E + 0	3.20E + 2	4.69E + 1	1.31E + 0	1.79E + 1
4.00E + 3	2.50E + 0	2.82E + 2	3.97E + 1	1.18E + 0	1.68E + 1
4.26E + 3	2.35E + 0	2.49E + 2	3.44E + 1	1.09E + 0	1.58E + 1
4.51E + 3	2.22E + 0	2.22E + 2	3.00E + 1	1.00E + 0	1.49E + 1
4.74E + 3	2.11E + 0	2.00E + 2	2.67E + 1	9.42E − 1	1.42E + 1
5.00E + 3	2.00E + 0	1.79E + 2	2.36E + 1	8.79E − 1	1.34E + 1
5.99E + 3	1.67E + 0	1.24E + 2	1.82E + 1	8.16E − 1	1.12E + 1
6.99E + 3	1.43E + 0	9.04E + 1	1.33E + 1	6.99E − 1	9.53E + 0
8.00E + 3	1.25E + 0	6.86E + 1	1.03E + 1	6.20E − 1	8.31E + 0
9.01E + 3	1.11E + 0	5.33E + 1	8.34E + 0	5.70E − 1	7.32E + 0
1.00E + 4	1.00E + 0	4.23E + 1	7.02E + 0	5.38E − 1	6.53E + 0
1.49E + 4	6.70E − 1	1.56E + 1	3.17E + 0	3.99E − 1	3.97E + 0
1.94E + 4	5.17E − 1	5.65E + 0	6.14E + 0	1.16E + 0	2.64E + 0

Table III. Nickel

ω (cm^{-1})	λ (μm)	$-\epsilon_1$	ϵ_2	n	k
1.80E + 2	5.56E + 1	9.07E + 3	2.12E + 4	8.37E + 1	1.27E + 2
2.00E + 2	5.00E + 1	9.28E + 3	1.84E + 4	7.52E + 1	1.22E + 2
2.20E + 2	4.55E + 1	9.18E + 3	1.58E + 4	6.75E + 1	1.17E + 2
2.40E + 2	4.17E + 1	8.91E + 3	1.37E + 4	6.08E + 1	1.12E + 2
2.60E + 2	3.85E + 1	8.51E + 3	1.18E + 4	5.50E + 1	1.07E + 2
2.80E + 2	3.57E + 1	8.06E + 3	1.03E + 4	5.00E + 1	1.03E + 2
3.00E + 2	3.33E + 1	7.62E + 3	8.95E + 3	4.55E + 1	9.84E + 1
3.20E + 2	3.13E + 1	7.16E + 3	7.85E + 3	4.16E + 1	9.43E + 1
3.40E + 2	2.94E + 1	6.70E + 3	6.88E + 3	3.81E + 1	9.03E + 1
3.60E + 2	2.78E + 1	6.23E + 3	6.10E + 3	3.53E + 1	8.65E + 1
3.80E + 2	2.63E + 1	5.80E + 3	5.44E + 3	3.28E + 1	8.29E + 1
4.00E + 2	2.50E + 1	5.40E + 3	4.88E + 3	3.06E + 1	7.96E + 1
4.20E + 2	2.38E + 1	5.05E + 3	4.43E + 3	2.89E + 1	7.67E + 1
4.40E + 2	2.27E + 1	4.74E + 3	3.98E + 3	2.69E + 1	7.39E + 1
4.60E + 2	2.17E + 1	4.42E + 3	3.64E + 3	2.56E + 1	7.12E + 1
4.80E + 2	2.08E + 1	4.16E + 3	3.31E + 3	2.41E + 1	6.88E + 1
5.00E + 2	2.00E + 1	3.89E + 3	3.05E + 3	2.30E + 1	6.65E + 1
5.50E + 2	1.82E + 1	3.33E + 3	2.51E + 3	2.05E + 1	6.13E + 1
6.00E + 2	1.67E + 1	2.90E + 3	2.14E + 3	1.87E + 1	5.71E + 1
6.50E + 2	1.54E + 1	2.57E + 3	1.84E + 3	1.72E + 1	5.35E + 1
7.00E + 2	1.43E + 1	2.30E + 3	1.61E + 3	1.59E + 1	5.06E + 1
7.50E + 2	1.33E + 1	2.10E + 3	1.40E + 3	1.46E + 1	4.80E + 1
8.00E + 2	1.25E + 1	1.91E + 3	1.21E + 3	1.32E + 1	4.57E + 1
8.50E + 2	1.18E + 1	1.74E + 3	1.05E + 3	1.21E + 1	4.34E + 1
9.00E + 2	1.11E + 1	1.59E + 3	9.09E + 2	1.10E + 1	4.13E + 1
9.50E + 2	1.05E + 1	1.44E + 3	7.89E + 2	1.00E + 1	3.93E + 1
1.00E + 3	1.00E + 1	1.31E + 3	6.96E + 2	9.33E + 0	3.73E + 1
1.10E + 3	9.09E + 0	1.08E + 3	5.66E + 2	8.36E + 0	3.39E + 1
1.20E + 3	8.33E + 0	9.05E + 2	4.84E + 2	7.79E + 0	3.11E + 1
1.30E + 3	7.69E + 0	7.79E + 2	4.21E + 2	7.29E + 0	2.89E + 1
1.40E + 3	7.14E + 0	6.78E + 2	3.66E + 2	6.79E + 0	2.69E + 1
1.50E + 3	6.67E + 0	5.93E + 2	3.19E + 2	6.35E + 0	2.52E + 1
1.60E + 3	6.25E + 0	5.18E + 2	2.86E + 2	6.08E + 0	2.36E + 1
1.70E + 3	5.88E + 0	4.59E + 2	2.60E + 2	5.86E + 0	2.22E + 1
1.80E + 3	5.56E + 0	4.09E + 2	2.38E + 2	5.66E + 0	2.10E + 1
1.90E + 3	5.26E + 0	3.65E + 2	2.20E + 2	5.53E + 0	1.99E + 1
2.00E + 3	5.00E + 0	3.27E + 2	2.06E + 2	5.45E + 0	1.89E + 1
2.25E + 3	4.44E + 0	2.57E + 2	1.79E + 2	5.30E + 0	1.69E + 1
2.50E + 3	4.00E + 0	2.12E + 2	1.60E + 2	5.19E + 0	1.54E + 1
2.75E + 3	3.64E + 0	1.77E + 2	1.42E + 2	5.01E + 0	1.42E + 1
3.00E + 3	3.33E + 0	1.51E + 2	1.29E + 2	4.87E + 0	1.32E + 1
3.25E + 3	3.08E + 0	1.31E + 2	1.17E + 2	4.73E + 0	1.24E + 1
3.50E + 3	2.86E + 0	1.14E + 2	1.07E + 2	4.60E + 0	1.16E + 1
3.75E + 3	2.67E + 0	1.01E + 2	9.82E + 1	4.46E + 0	1.10E + 1
4.00E + 3	2.50E + 0	9.07E + 1	9.08E + 1	4.34E + 0	1.05E + 1
4.25E + 3	2.35E + 0	8.03E + 1	8.38E + 1	4.23E + 0	9.91E + 0
4.50E + 3	2.22E + 0	7.11E + 1	7.91E + 1	4.20E + 0	9.42E + 0
4.75E + 3	2.10E + 0	6.55E + 1	7.55E + 1	4.15E + 0	9.10E + 0
5.00E + 3	2.00E + 0	6.09E + 1	7.06E + 1	4.02E + 0	8.78E + 0
6.00E + 3	1.67E + 0	4.44E + 1	5.63E + 1	3.69E + 0	7.62E + 0
7.00E + 3	1.43E + 0	3.42E + 1	4.61E + 1	3.41E + 0	6.77E + 0
8.01E + 3	1.25E + 0	2.69E + 1	3.95E + 1	3.23E + 0	6.11E + 0
9.00E + 3	1.11E + 0	2.16E + 1	3.49E + 1	3.12E + 0	5.60E + 0
1.00E + 4	1.00E + 0	1.83E + 1	3.11E + 1	2.99E + 0	5.21E + 0
1.50E + 4	6.65E − 1	1.05E + 1	1.82E + 1	2.29E + 0	3.97E + 0
2.00E + 4	4.99E − 1	6.05E + 0	1.15E + 1	1.87E + 0	3.09E + 0

match as nearly as possible both the magnitude and slope of the measured reflectance.

For Cu, we tried a constant low frequency wing correction as well as a Drude model extrapolation down to 1 cm^{-1} with a constant reflectance assumed below 1 cm^{-1}. The use of a Drude model low frequency wing changed the values of the optical constants at 180 cm^{-1} by at most 4% relative to the case of a constant wing. There was a <1% difference in the optical constants at 500 cm^{-1}, with the difference becoming correspondingly smaller at higher frequencies. The numbers in Table II were obtained using the Drude model low frequency wing correction described above.

For Ni, the use of a constant low frequency wing correction resulted in a pronounced downward hook in $-\epsilon_1$ at frequencies below ~300 cm^{-1}. Using the same type of Drude model low frequency wing correction we used for Cu almost completely removed the downward hook in $-\epsilon_1$. The numbers in Table III were obtained

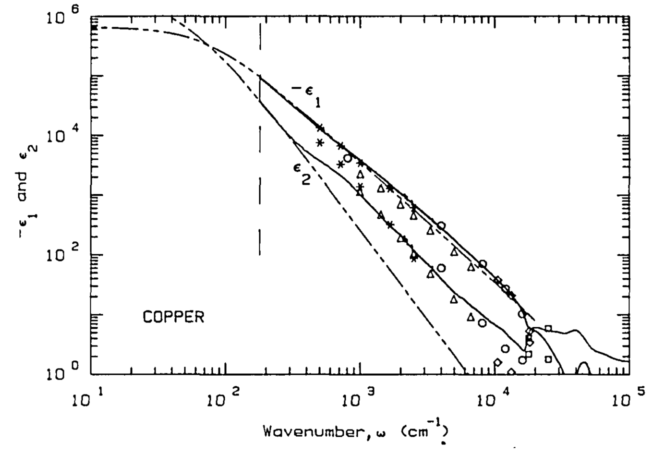

Fig. 1. Copper: $-\epsilon_1(\omega)$ and $\epsilon_2(\omega)$ vs frequency. The dashed lines are the Drude model fit. The solid lines are our data. Data from Ref. 1: Schulz, ◇ for both $-\epsilon_1$ and ϵ_2; Lenham and Treherne, * for $-\epsilon_1$ and ϵ_2; Robusto and Braunstein, □ for both; Hagemann *et al.*, ○ for both; and Dold and Mecke, △ for both. The dashed vertical line at 180 cm^{-1} marks the low frequency limit of our data.

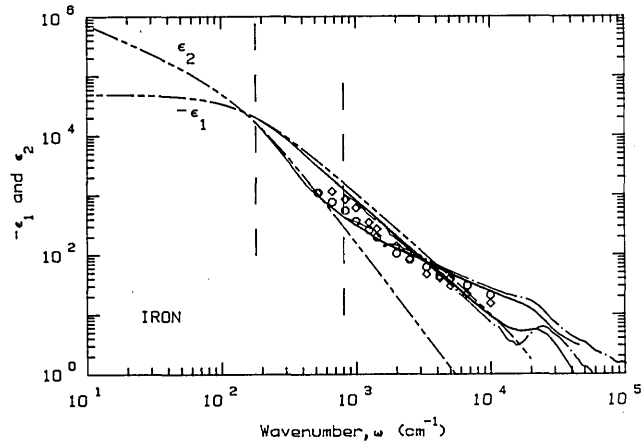

Fig. 2. Iron: $-\epsilon_1(\omega)$ and $\epsilon_2(\omega)$ vs frequency. The dashed lines are the Drude model fit. The solid lines are our data. The data from Ref. 2 are: Weaver *et al.*, dash-dot line for both $-\epsilon_1$ and ϵ_2; Bolotin *et al.*, ◇, for $-\epsilon_1$, and ○ for ϵ_2. The dashed vertical line at 180 cm^{-1} marks the low frequency limit of our data. The dashed vertical line at 807 cm^{-1} marks the low frequency limit of the Weaver *et al.* data.

using such a Drude model low frequency wing correction.

For Cu we found essentially perfect agreement in the 17,000–23,000-cm^{-1} range with the data of Weaver *et al.*[2] We arbitrarily used 20,000 cm^{-1} as a cutoff for our data and the higher frequency data from Weaver *et al.* as the first part of our high frequency wing correction. At the high frequency limit of the Weaver *et al.* data we assumed an inverse fourth-power dependence on the energy in electron volts. After this part of the high frequency wing fell to ~4×10^{-4} we assumed the reflectance remained constant at that value.

For Ni we found essentially perfect agreement in the 17,000–23,000-cm^{-1} range with the data of Lynch *et al.*[2] We arbitrarily used 20,000 cm^{-1} as a cutoff for our data and used the higher frequency data from Lynch *et al.* as the first part of our high frequency wing correction. At the high frequency limit of the Lynch *et al.* data we used the same wing correction described earlier for Cu.

For the high frequency wing correction for Fe we used the data of Moravec *et al.*[4] There was good agreement between our data and theirs with only a slight crossover between the two sets of data at 517 nm (~19,340 cm^{-1}). We used the Moravec *et al.* data as a high frequency wing correction starting at 517 nm. A constant low frequency wing correction was used for Fe.

The data of Weaver *et al.*[2] were converted from n, k, ϵ_1, and ϵ_2 vs energy (eV) to n, k, $-\epsilon_1$ and ϵ_2 vs both wave number (cm^{-1}) and wavelength (μm).

Figures 1–9 are plots of $-\epsilon_1(\omega)$ and $\epsilon_2(\omega)$ for nine metals. The dashed lines are calculated using Eqs. (3) and (4) using the Drude model parameters ω_τ and ω_p listed in Table I. Table I summarizes the results of our Drude model fit to the dielectric function of fourteen metals. Table I also includes the dc resistivity[5] ρ_0 and the optical resistivity ρ_{opt}. The optical resistivity ρ_{opt}

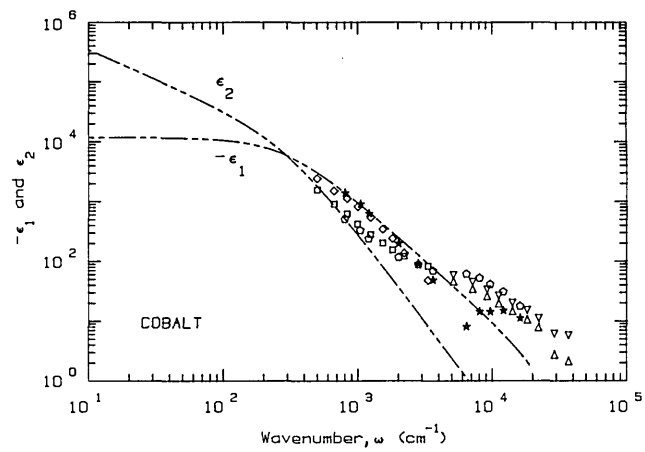

Fig. 3. Cobalt: $-\epsilon_1(\omega)$ and $\epsilon_2(\omega)$ vs frequency. The dashed lines are the Drude model fit. Data from Ref. 1: Johnson and Christy, △ for $-\epsilon_1$; X for ϵ_2; Weaver *et al.*, ★ for $-\epsilon_1$, ○ for ϵ_2.

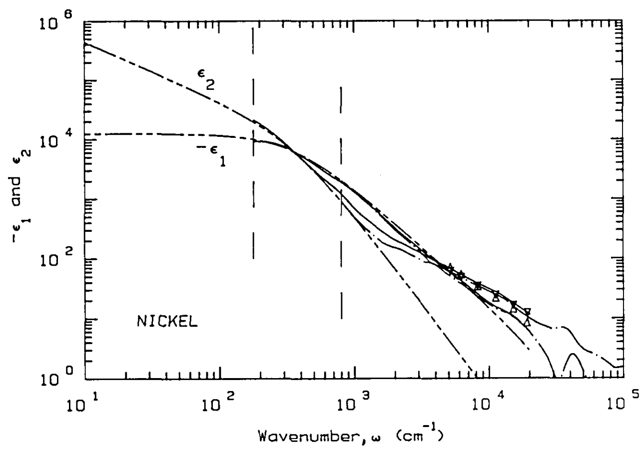

Fig. 4. Nickel: $-\epsilon_1(\omega)$ and $\epsilon_2(\omega)$ vs frequency. The dashed lines are the Drude model fit. The data from Ref. 1 are: Johnson and Christy, △ for $-\epsilon_1$ and X for ϵ_2. The solid line shows our data. The dashed vertical line at 180 cm^{-1} markes the low frequency limit of our data. The dash-dot lines are the data from Ref. 2: Lynch *et al.* The dashed vertical line at 807 cm^{-1} marks the low frequency limit of the Lynch *et al.* data.

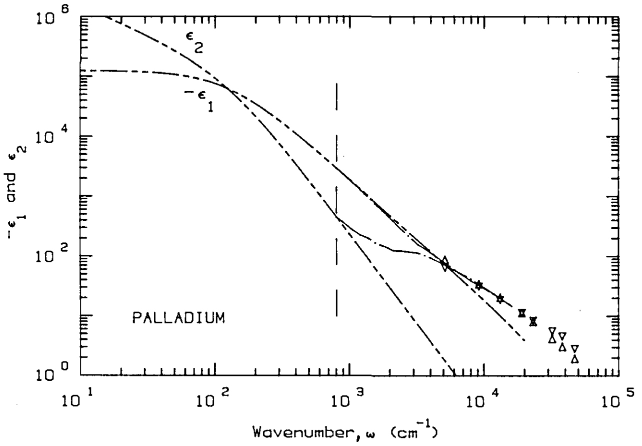

Fig. 5. Palladium: $-\epsilon_1(\omega)$ and $\epsilon_2(\omega)$ vs frequency. The dashed lines are the Drude model fit. The data from Ref. 1 are: Weaver and Benbow, dash–dot line for both $-\epsilon_1$ and ϵ_2; Johnson and Christy, Δ for $-\epsilon_1$ and X for ϵ_2. The dashed vertical line at 807 cm^{-1} marks the low frequency limit of the Weaver and Benbow data.

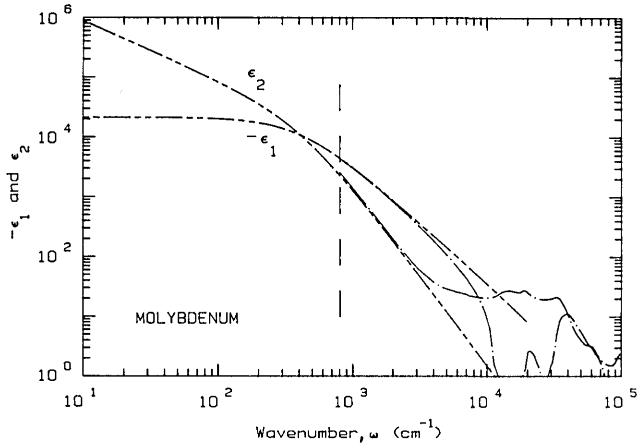

Fig. 8. Molybdenum: $-\epsilon_1(\omega)$ and $\epsilon_2(\omega)$ vs frequency. The dashed lines are the Drude model fit. The dash–dot lines are the data from Ref. 2: Weaver *et al.* The dashed vertical line at 807 cm^{-1} marks the low frequency limit of the Weaver *et al.* data.

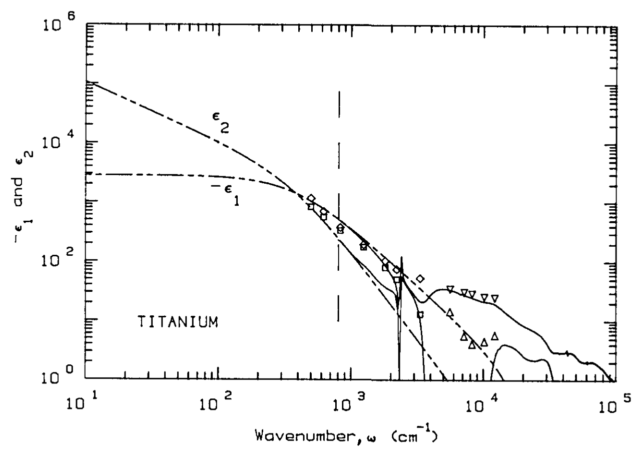

Fig. 6. Titanium: $-\epsilon_1(\omega)$ and $\epsilon_2(\omega)$ vs frequency. The dashed lines are the Drude model fit. The data from Ref. 1 are: Kirillova and Charikov (Opt. Spectrosc.), □ for $-\epsilon_1$ and ◇ for ϵ_2; Johnson and Christy, Δ for $-\epsilon_1$ and X for ϵ_2. The dash-dot lines are the data from Ref. 2: Lynch *et al.* The dashed vertical line at 807 cm^{-1} marks the low frequency limit of the Lynch *et al.* data.

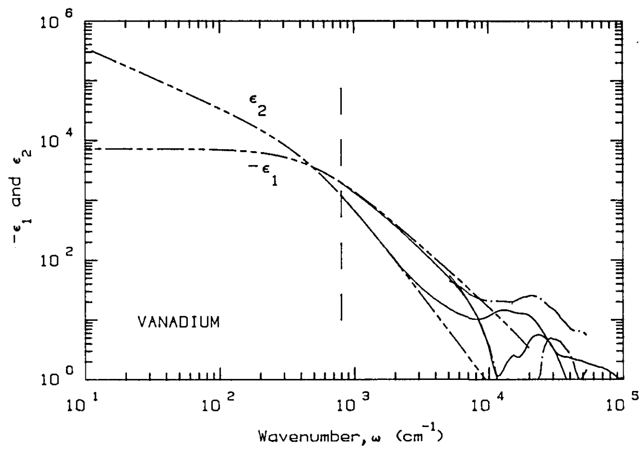

Fig. 9. Vanadium: $-\epsilon_1(\omega)$ and $\epsilon_2(\omega)$ vs frequency. The dashed lines are the Drude model fit. The solid lines are the data from Ref. 2: Weaver *et al.* The dash-dot lines are the data from Ref. 4: Johnson and Christy. The dashed vertical line at 807 cm^{-1} marks the low frequency limit of the Weaver *et al.* data.

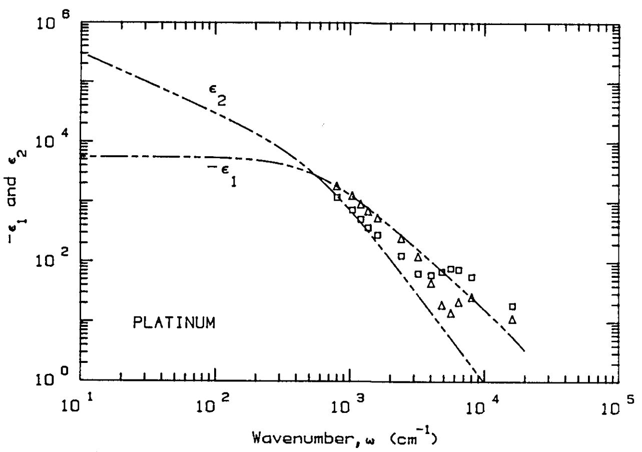

Fig. 7. Platinum: $-\epsilon_1(\omega)$ and $\epsilon_2(\omega)$ vs frequency. The dashed lines are the Drude model fit. The data from Ref. 1 are: Weaver *et al.*, ◇ for $-\epsilon_1$ and □ for ϵ_2.

in units of ohm cm was calculated from ω_τ and ω_p using

$$\rho_{\text{opt}} = \frac{60\omega_\tau}{\omega_p^2}\,. \tag{16}$$

Tables II, III, and IV present our new values of $-\epsilon_1$, ϵ_2, n, and k for Cu, Fe, and Ni. Table V presents the values of $-\epsilon_1$, ϵ_2, n, and k for Mo from Weaver *et al.*[2] Table VI presents the values of $-\epsilon_1$, ϵ_2, n, and k for V from Weaver *et al.*[2]

V. Summary

Infrared optical constants for Mo and V have been collected from the literature. New data for the optical constants Cu, Fe, and Ni are reported. The Drude model has been fit to the optical constants of the fourteen metals, Al, Co, Cu, Au, Fe, Pb, Mo, Ni, Pd, Pt, Ag, Ti, V, and W, to obtain ω_τ and ω_p. Our new data for

Table IV. Iron

ω (cm⁻¹)	λ (μm)	$-\epsilon_1$	ϵ_2	n	k
1.80E + 2	5.56E + 1	2.02E + 4	1.65E + 4	5.42E + 1	1.52E + 2
2.00E + 2	5.00E + 1	1.78E + 4	1.29E + 4	4.57E + 1	1.41E + 2
2.20E + 2	4.55E + 1	1.55E + 4	1.01E + 4	3.86E + 1	1.30E + 2
2.40E + 2	4.17E + 1	1.37E + 4	8.16E + 3	3.36E + 1	1.22E + 2
2.60E + 2	3.85E + 1	1.21E + 4	6.61E + 3	2.91E + 1	1.14E + 2
2.80E + 2	3.57E + 1	1.07E + 4	5.37E + 3	2.52E + 1	1.06E + 2
3.00E + 2	3.33E + 1	9.52E + 3	4.50E + 3	2.25E + 1	1.00E + 2
3.20E + 2	3.13E + 1	8.53E + 3	3.76E + 3	1.99E + 1	9.45E + 1
3.40E + 2	2.94E + 1	7.66E + 3	3.16E + 3	1.77E + 1	8.93E + 1
3.60E + 2	2.78E + 1	6.88E + 3	2.66E + 3	1.57E + 1	8.45E + 1
3.80E + 2	2.63E + 1	6.17E + 3	2.27E + 3	1.42E + 1	7.98E + 1
4.00E + 2	2.50E + 1	5.56E + 3	1.98E + 3	1.30E + 1	7.57E + 1
4.20E + 2	2.38E + 1	5.03E + 3	1.73E + 3	1.20E + 1	7.19E + 1
4.40E + 2	2.27E + 1	4.57E + 3	1.55E + 3	1.13E + 1	6.86E + 1
4.60E + 2	2.17E + 1	4.16E + 3	1.40E + 3	1.07E + 1	6.54E + 1
4.80E + 2	2.08E + 1	3.81E + 3	1.29E + 3	1.03E + 1	6.26E + 1
5.00E + 2	2.00E + 1	3.51E + 3	1.19E + 3	9.87E + 0	6.01E + 1
5.50E + 2	1.82E + 1	2.91E + 3	9.89E + 2	9.04E + 0	5.47E + 1
6.00E + 2	1.67E + 1	2.46E + 3	8.43E + 2	8.38E + 0	5.03E + 1
6.50E + 2	1.54E + 1	2.10E + 3	7.17E + 2	7.71E + 0	4.65E + 1
7.00E + 2	1.43E + 1	1.81E + 3	6.31E + 2	7.30E + 0	4.32E + 1
7.50E + 2	1.33E + 1	1.58E + 3	5.55E + 2	6.88E + 0	4.03E + 1
8.00E + 2	1.25E + 1	1.38E + 3	4.89E + 2	6.48E + 0	3.77E + 1
8.50E + 2	1.18E + 1	1.24E + 3	4.51E + 2	6.31E + 0	3.57E + 1
9.00E + 2	1.11E + 1	1.10E + 3	4.12E + 2	6.12E + 0	3.37E + 1
9.50E + 2	1.05E + 1	9.88E + 2	3.80E + 2	5.95E + 0	3.20E + 1
1.00E + 3	1.00E + 1	8.92E + 2	3.53E + 2	5.81E + 0	3.04E + 1
1.10E + 3	9.09E + 0	7.39E + 2	3.11E + 2	5.59E + 0	2.78E + 1
1.20E + 3	8.33E + 0	6.28E + 2	2.75E + 2	5.37E + 0	2.56E + 1
1.30E + 3	7.69E + 0	5.36E + 2	2.42E + 2	5.10E + 0	2.37E + 1
1.40E + 3	7.14E + 0	4.61E + 2	2.15E + 2	4.89E + 0	2.20E + 1
1.50E + 3	6.67E + 0	3.99E + 2	1.95E + 2	4.75E + 0	2.05E + 1
1.60E + 3	6.25E + 0	3.47E + 2	1.80E + 2	4.69E + 0	1.92E + 1
1.70E + 3	5.88E + 0	3.05E + 2	1.69E + 2	4.66E + 0	1.81E + 1
1.80E + 3	5.56E + 0	2.72E + 2	1.58E + 2	4.63E + 0	1.71E + 1
1.90E + 3	5.26E + 0	2.42E + 2	1.49E + 2	4.60E + 0	1.62E + 1
2.00E + 3	5.00E + 0	2.18E + 2	1.42E + 2	4.59E + 0	1.54E + 1
2.25E + 3	4.44E + 0	1.71E + 2	1.27E + 2	4.59E + 0	1.38E + 1
2.50E + 3	4.00E + 0	1.39E + 2	1.15E + 2	4.54E + 0	1.26E + 1
2.75E + 3	3.64E + 0	1.14E + 2	1.05E + 2	4.51E + 0	1.16E + 1
3.00E + 3	3.33E + 0	9.70E + 1	9.62E + 1	4.45E + 0	1.08E + 1
3.25E + 3	3.08E + 0	8.31E + 1	8.88E + 1	4.39E + 0	1.01E + 1
3.50E + 3	2.86E + 0	7.27E + 1	8.20E + 1	4.30E + 0	9.55E + 0
3.75E + 3	2.67E + 0	6.35E + 1	7.62E + 1	4.22E + 0	9.02E + 0
4.02E + 3	2.49E + 0	5.67E + 1	7.10E + 1	4.13E + 0	8.59E + 0
4.26E + 3	2.35E + 0	5.05E + 1	6.60E + 1	4.04E + 0	8.18E + 0
4.51E + 3	2.22E + 0	4.50E + 1	6.21E + 1	3.98E + 0	7.80E + 0
4.74E + 3	2.11E + 0	4.08E + 1	5.88E + 1	3.92E + 0	7.50E + 0
5.00E + 3	2.00E + 0	3.66E + 1	5.50E + 1	3.84E + 0	7.16E + 0
5.99E + 3	1.67E + 0	2.51E + 1	4.56E + 1	3.67E + 0	6.21E + 0
6.99E + 3	1.43E + 0	1.82E + 1	3.91E + 1	3.53E + 0	5.54E + 0
8.00E + 3	1.25E + 0	1.37E + 1	3.45E + 1	3.42E + 0	5.04E + 0
9.01E + 3	1.11E + 0	1.06E + 1	3.09E + 1	3.32E + 0	4.65E + 0
1.00E + 4	1.00E + 0	8.49E + 0	2.81E + 1	3.23E + 0	4.35E + 0
1.49E + 4	6.70E − 1	4.34E + 0	2.05E + 1	2.88E + 0	3.55E + 0
1.92E + 4	5.20E − 1	2.08E + 0	3.11E + 0	5.36E + 0	1.30E + 1

Cu caused a revision in the Drude model parameters presented in our previous tabulation.[1] The experimentally determined values of $-\epsilon_1$ and ϵ_2 are plotted along with the Drude model values for these quantities. This allows one to see how well the Drude model parametrizes the data for these metals. At the higher frequencies the free electron model is sometimes poor (exceptions[1] are Ag, Au, and Al) because of intraband effects or surface quality of samples.

Table V. Molybdenum: Weaver *et al.*[a]

ω (cm⁻¹)	λ (μm)	$-\epsilon_1$	ϵ_2	n	k
8.07E + 2	1.24E + 1	4.35E + 3	2.54E + 3	1.85E + 1	6.85E + 1
8.87E + 2	1.13E + 1	3.73E + 3	1.97E + 3	1.56E + 1	6.31E + 1
9.68E + 2	1.03E + 1	3.23E + 3	1.57E + 3	1.34E + 1	5.84E + 1
1.05E + 3	9.54E + 0	2.83E + 3	1.24E + 3	1.14E + 1	5.44E + 1
1.13E + 3	8.86E + 0	2.47E + 3	1.01E + 3	9.96E + 0	5.07E + 1
1.21E + 3	8.27E + 0	2.18E + 3	8.34E + 2	8.78E + 0	4.75E + 1
1.29E + 3	7.75E + 0	1.94E + 3	6.92E + 2	7.74E + 0	4.47E + 1
1.37E + 3	7.29E + 0	1.73E + 3	5.82E + 2	6.91E + 0	4.22E + 1
1.45E + 3	6.89E + 0	1.55E + 3	4.95E + 2	6.21E + 0	3.99E + 1
1.53E + 3	6.53E + 0	1.40E + 3	4.25E + 2	5.61E + 0	3.79E + 1
1.61E + 3	6.20E + 0	1.27E + 3	3.67E + 2	5.10E + 0	3.60E + 1
1.69E + 3	5.90E + 0	1.15E + 3	3.19E + 2	4.65E + 0	3.43E + 1
1.77E + 3	5.64E + 0	1.05E + 3	2.79E + 2	4.26E + 0	3.27E + 1
1.86E + 3	5.39E + 0	9.65E + 2	2.45E + 2	3.92E + 0	3.13E + 1
1.94E + 3	5.17E + 0	8.86E + 2	2.17E + 2	3.61E + 0	3.00E + 1
2.02E + 3	4.96E + 0	8.15E + 2	1.93E + 2	3.36E + 0	2.88E + 1
3.07E + 3	3.26E + 0	3.37E + 2	6.28E + 1	1.70E + 0	1.84E + 1
4.03E + 3	2.48E + 0	1.82E + 2	3.71E + 1	1.37E + 0	1.36E + 1
5.00E + 3	2.00E + 0	1.07E + 2	2.87E + 1	1.38E + 0	1.04E + 1
5.97E + 3	1.68E + 0	6.97E + 1	2.54E + 1	1.51E + 0	8.38E + 0
8.07E + 3	1.24E + 0	2.74E + 1	2.17E + 1	1.94E + 0	5.58E + 0
1.05E + 4	9.54E − 1	6.34E + 0	2.07E + 1	2.77E + 0	3.74E + 0
1.54E + 4	6.53E − 1	−1.17E + 0	2.68E + 1	3.74E + 0	3.58E + 0
2.02E + 4	4.96E − 1	2.61E + 0	2.50E + 1	3.36E + 0	3.73E + 0

[a] Ref. 2, p. 148.

Table VI. Vanadium: Weaver *et al.*[a]

ω (cm⁻¹)	λ (μm)	$-\epsilon_1$	ϵ_2	n	k
8.07E + 2	1.24E + 1	1.94E + 3	1.18E + 3	1.28E + 1	4.59E + 1
9.68E + 2	1.03E + 1	1.43E + 3	7.47E + 2	9.51E + 0	3.90E + 1
1.29E + 3	7.75E + 0	8.69E + 2	3.47E + 2	5.77E + 0	3.00E + 1
1.61E + 3	6.20E + 0	5.75E + 2	1.86E + 2	3.90E + 0	2.43E + 1
1.94E + 3	5.17E + 0	4.05E + 2	1.15E + 2	2.82E + 0	2.03E + 1
2.90E + 3	3.44E + 0	1.75E + 2	4.10E + 1	1.54E + 0	1.33E + 1
3.87E + 3	2.58E + 0	9.39E + 1	2.33E + 1	1.19E + 0	9.77E + 0
5.16E + 3	1.94E + 0	4.85E + 1	1.50E + 1	1.07E + 0	7.04E + 0
6.13E + 3	1.63E + 0	3.10E + 1	1.23E + 1	1.08E + 0	5.67E + 0
7.26E + 3	1.38E + 0	1.88E + 1	1.06E + 1	1.18E + 0	4.50E + 0
8.07E + 3	1.24E + 0	1.26E + 1	1.02E + 1	1.34E + 0	3.80E + 0
8.87E + 3	1.13E + 0	8.06E + 0	1.04E + 1	1.60E + 0	3.26E + 0
1.01E + 4	9.92E − 1	3.31E + 0	1.16E + 1	2.09E + 0	2.77E + 0
1.49E + 4	6.70E − 1	2.43E + 0	1.38E + 1	2.41E + 0	2.87E + 0
2.02E + 4	4.96E − 1	4.36E + 0	1.18E + 1	2.02E + 0	2.91E + 0
5.16E + 3	1.94E + 0	5.46E + 1	4.41E + 1	2.79E + 0	7.90E + 0
6.21E + 3	1.61E + 0	3.25E + 1	3.51E + 1	2.77E + 0	6.34E + 0
7.18E + 3	1.39E + 0	1.96E + 1	2.72E + 1	2.64E + 0	5.15E + 0
8.23E + 3	1.22E + 0	1.15E + 1	2.34E + 1	2.70E + 0	4.33E + 0
9.20E + 3	1.09E + 0	6.05E + 0	2.17E + 1	2.87E + 0	3.78E + 0
1.05E + 4	9.84E − 1	3.61E + 0	2.06E + 1	2.94E + 0	3.50E + 0
1.52E + 4	6.59E − 1	−1.01E + 0	2.01E + 1	3.25E + 0	3.09E + 0
2.02E + 4	4.96E − 1	−4.74E + 0	2.56E + 1	3.92E + 0	3.26E + 0
2.52E + 4	3.97E − 1	2.69E + 0	2.14E + 1	3.07E + 0	3.48E + 0
3.02E + 4	3.32E − 1	4.75E + 0	1.53E + 1	2.37E + 0	3.22E + 0
3.52E + 4	2.84E − 1	3.96E + 0	1.02E + 1	1.87E + 0	2.73E + 0
4.02E + 4	2.49E − 1	2.68E + 0	7.33E + 0	1.60E + 0	2.29E + 0
4.52E + 4	2.21E − 1	1.26E + 0	6.45E + 0	1.63E + 0	1.98E + 0
5.02E + 4	1.99E − 1	1.14E + 0	6.29E + 0	1.62E + 0	1.94E + 0
5.32E + 4	1.88E − 1	1.45E + 0	5.59E + 0	1.47E + 0	1.90E + 0

[a] Ref. 2, p. 50.

The optical resistivities ρ_{opt} have been computed [using Eq. (16)] and compared with the handbook values of the dc resistivities ρ_0. The ratios of these two resistivities are of the order of unity for Al, Au, Fe, Pb, Mo, Ag, Ti, and V. We suggest, however, that new measurements of ρ_0 would be useful for a number of these fourteen metals.

We want to thank M. Milham and E. Steubing for encouraging and supporting this work. We would also like to express our appreciation to C. A. Ward (Krebs) for helping to lay the groundwork for this endeavor.

This work was partially supported by grant DAAA-15-85-K-0004 (M. Milham).

References

1. M. A. Ordal, L. L. Long, R. J. Bell, S. E. Bell, R. R. Bell, R. W. Alexander, and C. A. Ward, "Optical Properties of the Metals Al, Co, Cu, Au, Fe, Pb, Ni, Pt, Ag, Ti, and W in the Infrared and Far Infrared," Appl. Opt. **22**, 1099 (1983).
2. J. H. Weaver, C. Krafka, D. W. Lynch, and E. E. Koch, *Physics Data, Optical Properties of Metals, Part I: The Transition Metals* (Fachinformationszentrum, 7514 Eggenatein-Leopoldshafen 2, Karlsruhe, Federal Republic of Germany, 1981).
3. P. B. Johnson and R. W. Christy, "Optical Constants of Transition Metals: Ti, V, Cr, Mn, Fe, Co, Ni, and Pd," Phys. Rev. **9**, 5056 (1974).
4. T. J. Moravec, J. C. Rife, and R. N. Dexter, "Optical Constants of Nickel, Iron, and Nickel-Iron Alloys in the Vacuum Ultraviolet," Phys. Rev. B **13**, 3297 (1976).
5. J. Babiskin and J. R. Anderson, Eds., *American Institute of Physics Handbook* (McGraw-Hill, New York, 1972), pp. 9-39, 9-40.
6. S. Perkowitz, G. L. Carr, B. Subramaniam, and B. Mitrovic, "Far-infrared Determination of Scattering Behavior and Plasma Frequency in V_3Si, Nb_3Ge, and Hb," Phys. Rev. B **32**, 153 (1985).

Patter *continued from page 4472*

Laser schlieren crystal-growth imager

A crystal can be observed as it grows from a melt with the aid of laser schlieren imaging. The observation method allows the entire perimeter of the growing crystal to be inspected. Isolated crystal facets can be examined, and convection flows and temperature and concentration gradients are revealed. The method does not require contact with or proximity to the crystal. The schlieren technique detects density gradients in a fluid. Collimated light passes through the crystal-growth medium and is focused on a knife-edge. The image of the growth medium and crystal is projected onto a screen (see Fig. 17).

In general, light traveling through a nonuniform medium is refracted in the direction of an increasing refractive-index gradient (which is usually in the direction of increasing density). In the liquid around a growing crystal, material is continuously being absorbed from the liquid by the crystal. Thus, the density of the liquid increases with distance from the solid/liquid interface. Light traveling parallel to the interface is thus refracted away from the growing solid surface. In the case of a dissolving crystal, material is being added to the solution. The density of melt thus increases toward the dissolving crystal face. Light traveling parallel to the face is thus refracted toward the face.

Therefore, in the schlieren system of the figure, the growing crystal will create a bright band at the image of the upper face of the crystal and a dark band at the image of the lower face. If the crystal is dissolving, the dark band will be at the image of the upper face, and the bright band will be at the image of the lower face. If the crystal is neither growing nor dissolving, only pale bands will appear. To examine the sides of the crystal instead of the top and bottom for growth or dissolution, one should rotate the knife-edge by 90° around the optical axis. The relative positions of the light and dark bands can also be reversed by rotating the knife-edge 180° around the optical axis from the present position.

This work was done by Robert B. Owen and Mary H. Johnston of Marshall Space Flight Center. This invention is owned by NASA, and a patent application has been filed. Inquiries concerning license for its commercial development should be addressed to the Patent Counsel, Marshall Space Flight Center. Mail Code CC-01, Ala. 35812. Refer to MFS-28060.

Fig. 17. Beam of laser light is projected through a growth medium such as a molten material containing a crystal of the same material, then over a knife-edge, and onto a screen. This method will be used to monitor growth and dissolution of a triglycine sulfate crystal in microgravity aboard Spacelab III.

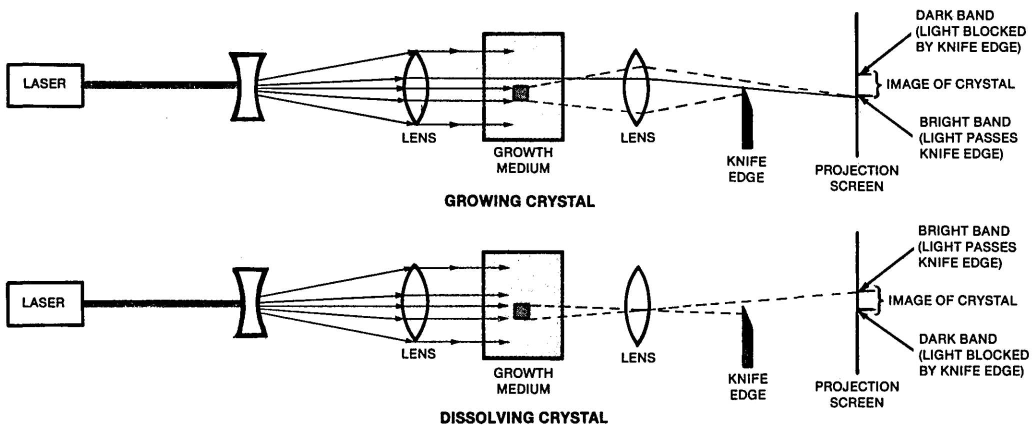

continued on page 4503